Langevin Network Model of Myosin†

Benjamin T. Miller, Wenjun Zheng,‡ Richard M. Venable, Richard W. Pastor, and Bernard R. Brooks*

Laboratory of Computational Biology, National Heart, Lung and Blood Institute, National Institutes of Health, Bethesda, Maryland 20892

Received: September 1, 2007; In Final Form: November 6, 2007

Langevin mode theory and the coarse-grained elastic network model (ENM) for proteins are combined to yield the Langevin network model (LNM). Hydrodynamic radii of 6 Å were assigned to each α-carbon on the basis of matching experimental translational and rotational diffusion constants of lysozyme, myoglobin, and hemoglobin with those calculated using a rigid body bead model with hydrodynamic interactions described by the Rotne−Prager tensor. LNM analysis of myosin II indicates that all ENM-like modes are overdamped at water viscosities. The low-frequency LNM modes in the pre-power stroke structure (PDB code: 1VOM) are substantially less mixed than the corresponding modes of the post-power stroke structure (1Q5G). Results from a four-bead model of the myosin "lever arm" indicate that coupling between modes increases as the array departs from linearity and are consistent with the results for 1VOM and 1Q5G. The decay times for all overdamped Langevin modes are shorter than the calculated rotational tumbling times found for lysozyme and myosin.

1. Introduction

Biomolecular processes generally take place in a viscous environment within the cell, and therefore, the ability to model the effect of solvent friction on proteins is a useful step to understanding these processes. However, many important proteins are too large for current computers to simulate with all-atom Langevin dynamics or molecular dynamics with explicit or implicit solvent models. One such example is the skeletal muscle protein myosin II. How is the behavior of myosin affected by friction? One way to begin to address these questions is by varying the viscosity of the solvent environment. For example, experiments where the normal H_2O environment has been replaced with D_2O, which has a 25% greater viscosity, demonstrate a 40−50% slowing of action and an increased rate of ATP hydrolysis, resulting in a reduced efficiency.[1] Another way to address these questions is to examine the system using a Langevin mode analysis in which the flexibility of the macromolecule is coupled with a friction tensor representing the viscosity of the local environment.

Previous work has been done to incorporate the effects of friction into vibrational analysis. For example, Kneller examined Langevin motion in macromolecules using a coarse-grained scheme and demonstrated that incorporating friction at the atomic level is not the equivalent to broadening the lines of the corresponding normal mode spectrum.[2] Lange and Grubmüller developed a collective Langevin dynamics (CLD) method in which a reduced dimension approach is used to evolve the dynamics of the system.[3] Erkip and Erman used the Langevin equation to analyze the contributions of solvent friction to the motion of a protein described by the Gaussian network model.[4]

The role of myosin within a muscle is to transform the energy released by ATP hydrolyzation into mechanical work. Himmel et al.[5] summarized the basic structural details of scallop myosin collected from crystallographic sources and proposed a mechanism relating structure and function. The myosin motor domain consists of four rigid subdomains, of which the converter and its C-terminal extension (the lever arm) are particularly important. The rotational motion or "power stroke" releases the mechanical energy gained from breaking the phosphate bond to produce motion along the bound actin. The efficiency of this process has been estimated to be ∼40%.[6] Two conformational states found by structural studies are the pre-power-stroke state, in which the lever arm is in the up position (Protein Data Bank[7] code 1VOM), and the post-rigor weak actin-binding state, in which the lever arm is in the down position (PDB code: 1MMA). Subsequently, 1Q5G, a nucleotide-free myosin structure in the rigorlike state that can bind strongly to actins was solved by Reubold et al.[8] Figure 1 shows these three structures of myosin (lysozyme (PDB code 8LZM), used for testing in the present study, is also included). Rüegg et al. report that for rabbit fast skeletal muscle myosin II, the working stroke moves ∼5 nm and completes within ∼5 ms.[9]

Myosin and related systems have been well-studied using the elastic network model (ENM).[10−16] The ENM is a coarse-grained model in which residues are represented by a single center at the C_α position and proximal residues are connected by harmonic springs. This approach limits the computational cost and complexity of the calculation and reduces the effect of noise from a calculation at full atomic detail (i.e., the sensitivity of the results to minor conformational differences). Zheng et al. recently studied the transition between the myosin structures 1VOM and 1Q5G using a mixed ENM potential.[17] Here, we combine the Langevin mode theory of Lamm and Szabo[14] and ENM to formulate the Langevin network model (LNM). We then use LNM to analyze the behavior of myosin

† Part of the "Attila Szabo Festschrift".

* To whom correspondence should be addressed. E-mail brb@nih.gov.
‡ Present address: Department of Physics, University at Buffalo, 239 Fronczak Hall, Buffalo, NY 14260.

10.1021/jp077042v
Published on Web 03/01/2008

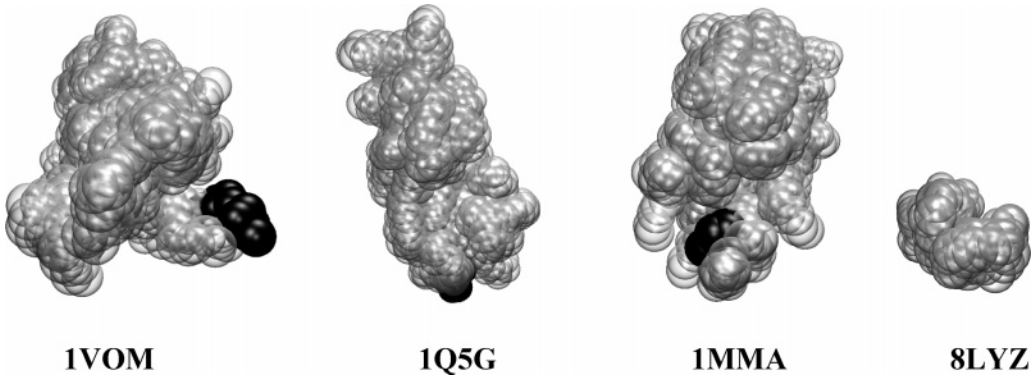

Figure 1. Representations of the myosin structures 1VOM, 1Q5G, 1MMA, and lysozyme 8LYZ using the coarse grained model with a 6.0 Å bead radius. Residues in the converter of myosin are depicted in dark gray, and the others are semitransparent. Images were generated using VMD[33] and Raster3D.[34]

as the solvent friction increases from 0 (i.e., standard ENM calculations) to 1 cP (that of water at room temperature).

By way of outline, the Methods Section reviews the Langevin mode method (2.1) and then defines the force matrix (derived from the elastic network model) (2.2) and the friction matrix (derived from a bead model treatment of hydrodynamic interaction) (2.3) and describes the approach used to assess overlap between different modes (2.4). The Results Section begins with the determination of hydrodynamic radii for the α-carbons (C_α) (3.1) and testing of the LNM method on lysozyme and proceeds to a detailed study of myosin structures 1VOM and 1Q5G (3.2). Section 3.3 presents results on four-bead model in linear and bent arrangements to illustrate geometry dependence of mixing of LNM modes and provides insight into differences in the dynamics of the low-frequency normal modes in the pre- and post-power-stroke structures of myosin.

2. Methods

2.1. Overview of the Langevin Mode Method. Standard normal-mode analysis formulates Newton's equations of motion in matrix form employing the assumption that the system can be well-represented in the low-temperature harmonic limit. Diagonalizing a Hessian-based matrix yields eigenvalues and eigenvectors that define oscillatory motion of the system being studied in the harmonic limit. The Langevin mode theory developed by Lamm and Szabo[18] expands this method by adding a frictional force conformant to the Langevin equation:

$$-V'(\mathbf{q}) - \zeta\dot{\mathbf{q}} + \mathbf{R}(t) = \mathbf{m}\ddot{\mathbf{q}} \tag{1}$$

where V is the potential energy function, $\mathbf{q}$ is the position vector of the systems, $\dot{\mathbf{q}}$ is the velocity vector, $\ddot{\mathbf{q}}$ is the acceleration, ζ is the 3N × 3N friction matrix, $\mathbf{m}$ is the 3N × 3N diagonal mass matrix, and $\mathbf{R}(t)$ is the vector of random forces as a function of time, which are subject to the following constraints:

$$\langle R_i(t)\rangle = 0$$

$$\langle R_i(t)\cdot R_j(t')\rangle = \frac{2\zeta_{ij}\delta(t-t')}{k_B T} \tag{2}$$

where i and j are atom indices, k_B is Boltzmann's constant, T is temperature, and $\delta(t - t')$ is the Kronecker delta.

Following Kottalam and Case,[19] a first-order Taylor series expansion of the Langevin equation describes the behavior of the system in terms of an oscillatory motion around a minimum position, q^0. To simplify, α_i is set to the root mass weighted deviation from q^0:

$$\alpha_i = \sqrt{m_i}\,(q_i - qi^0) \tag{3}$$

Substituting eq 3 into eq 1 yields

$$\ddot{q}_i = \sum_{j=1}^{3N}\left(-\left[\frac{1}{\sqrt{m_i m_j}}\left(\frac{\partial^2 V}{\partial q_i \partial q_j}\right)\right]\alpha_i - \left[\frac{\zeta_{ij}}{\sqrt{m_i m_j}}\right]\dot{q}_i + R_i(t)\right) \tag{4}$$

If $\zeta_{ij} = 0$ for all i and j, then there is zero frictional force on the system, and eq 4 reduces to the usual gas-phase normal-mode equation.

Writing eq 4 in matrix form gives

$$\begin{bmatrix}\dot{\boldsymbol{\alpha}}\\ \ddot{\mathbf{q}}\end{bmatrix} = \begin{bmatrix}\mathbf{0} & \mathbf{I}\\ -\mathbf{F} & -\boldsymbol{\gamma}\end{bmatrix}\begin{bmatrix}\boldsymbol{\alpha}\\ \dot{\mathbf{q}}\end{bmatrix} + \begin{bmatrix}\mathbf{0}\\ \mathbf{R(t)}\end{bmatrix} = [\mathbf{A}]\begin{bmatrix}\boldsymbol{\alpha}\\ \dot{\mathbf{q}}\end{bmatrix} + \begin{bmatrix}\mathbf{0}\\ \mathbf{R(t)}\end{bmatrix} \tag{5}$$

where $\mathbf{F}$ is the 3N × 3N mass-weighted second derivative Hessian matrix, $\mathbf{I}$ is the 3N × 3N identity matrix, and γ is the 3N × 3N mass-weighted matrix of the ζ_{ij} terms. This formulation explicitly decomposes the problem into positional and velocity components. As Lamm and Szabo show,[18] to solve for $\boldsymbol{\alpha}$ and $\dot{\mathbf{q}}$, it is only necessary to solve the eigenvalue problem for the 6N × 6N matrix on the right-hand side of eq 5, denoted $\mathbf{A}$.

With the $\mathbf{F}$ and $\boldsymbol{\gamma}$ matrices in place, $\mathbf{A}$ is diagonalized and the eigenvalues and eigenvectors are computed using the DGEEV LAPACK routine. Since $\mathbf{F}$ and $\boldsymbol{\gamma}$ are nonnegative definite matrices, the eigenvalues and eigenvectors of $\mathbf{A}$ take a special form, as described by Lamm and Szabo. Because $\mathbf{A}$ is not symmetric, the eigenvalues may be complex; however, the real parts must always be nonpositive. Imaginary eigenvalues appear in complex conjugate pairs. If an eigenvalue is complex, the corresponding mode is underdamped; the inverse of the real component is the relaxation time, and the imaginary part is the oscillation frequency. If a mode is real it has only the damping part and no oscillatory part. Furthermore, by eq 5, the top 3N components of the eigenvectors represent the positional deformation along the mode and the bottom 3N elements represent velocities. The bottom 3N elements of the eigenvector are thus equal to the top 3N multiplied by the eigenvalue.

Due to the dimension of **A**, there are twice as many Langevin modes as degrees of freedom in the system. Although the Langevin modes, like classic normal modes, form a linearly independent basis set, they cannot be mutually orthogonal, and therefore, some of them must be coupled. In fact, pairs of underdamped modes are complex conjugates of one another. As friction is increased, the magnitude of the damping portions of these vectors increases while that of the oscillatory part decreases, and the modes begin to couple. Eventually, the pair of modes becomes overdamped and the real parts of the eigenvalues diverge. There are methods, discussed below, of evaluating the exact magnitude of the change in the motion represented by the mode as this process occurs.

2.2. Calculation of the Force Matrix. Constructing **A** requires the calculation of both the **F** and γ matrices. For this study, the potential used is that of the elastic network model developed by Tirion.[20] This is a spring potential given by

$$E(q_i,q_j) = \frac{C}{2}(|\mathbf{r_{ij}}| - |\mathbf{r_{ij}}^{\mathbf{0}}|)^2 \qquad (6)$$

where C is the force constant and the three-dimensional vector $\mathbf{r_{ij}}$ is defined as $\mathbf{q_i} - \mathbf{q_j}$. Rather than calculating this for each atom in the system, the model is coarse grained with only α-carbons (C_α) considered.

The calculations of the ENM potentials and second derivative matrix for the target system were performed using CHARMM, version c34a2.[21] The spring potential was implemented using the distance restraint functionality of the program after removing all atoms other than α-carbons from the system. Two different force constants were used for myosin: 4.0 kcal/mol/Å^2 for the short range interactions of neighboring C_α (within 4.5 Å) and 0.4 kcal/mol/Å^2 for pairs more than 4.5 Å but less than the cutoff value of 10 Å. No springs connected C_α more than 10 Å apart. Likewise, short and long-range force constants of 5.0 and 0.5 kcal/mol/Å^2 for lysozyme were used. These force constants were determined on the basis of the fitting of B-factors.[22]

2.3. Calculation of the Friction Matrix. The second matrix necessary to perform the Langevin modes calculation is γ, the friction matrix. Kottalam and Case[19] report that for crambin and the DNA duplex d(CpGpCpGpCpG)$_2$, hydrodynamic shielding can significantly affect the observed relaxation times of the Langevin modes. The Rotne−Prager tensor accounts for the shielding and is obtained by defining a matrix **T**, consisting of 3 × 3 blocks $\mathbf{T_{ij}}$ describing the hydrodynamic interaction between particles i and j, and inverting. Each element of the 3 × 3 blocks of $\mathbf{T^{-1}}$ is then divided by $\sqrt{m_i m_j}$.

The individual bead friction constants (ζ_i) were evaluated from Stokes Law,

$$\zeta_i = 6\pi\eta a_i \qquad (7)$$

where η is the solvent viscosity and a is the hydrodynamic radius. All C_α were assigned the same hydrodynamic radius, which was obtained from fitting experimental translational[23−26] and rotational[27−28] constants using the bead model formalism of Garcia de la Torre and Bloomfield[29] as implemented by Venable and Pastor.[30] As shown in Section 3.1, bead radii providing reasonable fits to the experimental data are greater than the C_α−C_α bond distance; that is, the beads overlap. This overlap leads to instabilities when the Oseen tensor is used to describe hydrodynamic interaction and necessitates the use of the Rotne−Prager tensor[31] for $\mathbf{T_{ij}}$.

$$\begin{aligned}
\mathbf{T_{ij}} &= (6\pi\eta a_i)^{-1}\mathbf{I} \qquad \text{when } i = j \\
&= (8\pi\eta|r_{ij}|)^{-1}\left[\mathbf{I} + \frac{r_{ij}r_{ij}^t}{|r_{ij}|^2}\right] + \\
&\qquad (8\pi\eta|r_{ij}|^3)^{-1}(a_i + a_j)\left[\frac{1}{3}\mathbf{I} - \frac{r_{ij}r_{ij}^t}{|r_{ij}|^2}\right] \\
&\qquad \text{when } i \neq j \text{ and } r_{ij} \geq a_i + a_j \\
&= (6\pi\eta a_i)^{-1}\left[\left(1 - \frac{9|r_{ij}|}{32}\right)\mathbf{I} + \frac{3(r_{ij}r_{ij}^t)}{32a_i|r_{ij}|}\right] \\
&\qquad \text{when } i \neq j \text{ and } r_{ij} < 2a_i \ (a_i \text{ must equal } a_j) \qquad (8)
\end{aligned}$$

where r_{ij}^t is the adjoint of r_{ij} and **I** is the 3 × 3 identity matrix. Custom code was used to compute **T** and $\mathbf{T^{-1}}$, the latter being calculated using the DGETRF and DGETRI LAPACK routines, which invert the matrix by means of its LU factorization.

2.4. Calculation of Overlap Scores of Modes. Brooks et al.[32] define an overlap score to compare modes by averaging the dot products of various modes. The dot product of two vectors normalized to length 1 ranges from −1 to 1. To simplify matters, the absolute value of this overlap is given so that two modes with a dot product of 1 are identical and two modes with a dot product of 0 are completely orthogonal to one another. The normal modes calculated by CHARMM are a set of mutually orthogonal vectors. Therefore, given an arbitrary vector, the sum of the squares of the dot products of this vector with each of the normal mode vectors must equal 1 (because the normal modes span the set of possible motions of the structure). Therefore, it is possible to determine how closely many modes must be combined to recapture any motion. Brooks et al. make use of this fact to compare normal modes calculated via various mechanisms. It is desirable to develop a similar methodology for comparing Langevin modes to see how the motion of the structure changes as friction increases.

As described above, the Langevin modes are coupled with one another at high friction. Hence, although it is still possible to compare two Langevin modes, the sum of the squares of the dot products of a given vector versus an entire set of Langevin modes will yield a result greater than 1. This scheme is thus unusable for comparing how much of the total range of motion is captured in any particular vector. To use the Langevin modes for this task, it is necessary to simplify them. Fortunately, the top and bottom halves of the vectors are related as described above. For critically damped and overdamped, either half may be taken and renormalized to give a length 3N vector that can be compared directly with ENM normal mode vectors. For underdamped modes, the two halves each contain complex vectors yielding information about both the damping and oscillatory motions. We take half of the vector, renormalize it, split the vector into its real and imaginary components, and compare these with the ENM normal mode vectors to determine how much of the motion is captured in the oscillatory and real parts of the vector. An example of this analysis for a very simple system is given in Section 3.3. It is also possible to extrapolate the zero friction Langevin modes from the ENM modes and compare these with higher-frequency LNM modes directly. This has been done to generate the overlap scores with lysozyme and myosin.

Results

3.1. Determination of C_α Hydrodynamic Radius. Translational and rotational diffusion constants were evaluated for

TABLE 1: Experimental and Calculated Translational Diffusion Constants (10^{-6} cm^2/s), Rotational Relaxation Times (ns), and Protein Data Bank Codes for Structures Used

	$D_{20,w}$		τ_{iso}		
protein	expt	calc[a]	expt	calc[a,b]	PDB codes
lysozyme	1.07[c]	1.09	5.7[d]	5.5	1E8L, 2VB1, 8LYZ
myoglobin[e,f]	1.02[e]	1.02	9.7[f]	11.1	1DWR, 1WLA, 1YMB
hemoglobin[e,f]	0.69[e]	0.66	37.7[f]	38.7	1GXZ, 2DN2, 2H35

[a] Average from each of the 3 PDB coordinate sets indicated. [b] Scaled to experimental temperature and viscosity (1.1 cP for Mb and Hb; assumed to be that of pure water for lys). [c] Average of values from refs 23−25. [d] Ref 27. [e] Ref 25. [f] Ref 28.

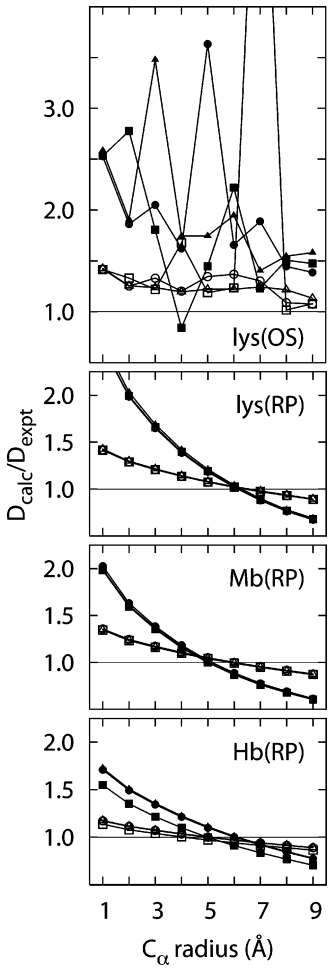

Figure 2. Ratio of calculated and experimental translational (open symbols) and rotational (filled symbols) diffusion constants for lysozyme (lys), myoglobin (Mb), and hemoglobin (Hb) versus hydrodynamic radius of the C_α carbon. Values in top panel for Oseen tensor (OS); all others for Rotne−Prager (RP) tensor. Unique symbols are used for each structure of a given protein.

lysozyme (lys), myoglobin (Mb), and hemoglobin (Hb) for C_α radii varying from 1 to 9 Å. Three structures from the Protein Data Bank were used for each protein (Table 1). The top two panels of Figure 2 compare results for lys obtained from the Oseen and Rotne−Prager (R−P) tensors, respectively. At a bead radius of 1 Å D_{calc}/D_{expt}, the ratio of calculated and experimental diffusion constants for translation (open symbols) and rotation (closed symbols) are nearly identical, as expected when there is no overlap between hydrodynamic beads (the distance between neighboring C_α in proteins is 3.8 Å). However, the calculated diffusion constants are too high, indicating that larger bead radii are required. Here, the results for the Oseen tenor

TABLE 2: Translational Diffusion Constants (10^{-6} cm^2/s) and Rotational Relaxation Times (ns) at 20 °C for Lysozyme and Myosin (1VOM), Where C_α with Accessible Surface below the Cutoff (Å^2) Were Assigned a Zero Friction Constant[a]

	lysozyme			myosin		
cutoff	N	$D_{20,w}$	τ_{iso}	N	$D_{20,w}$	τ_{iso}
no cutoff	129	1.09	8.10	730	0.56	61.4
0	92	1.10	7.92	427	0.56	60.8
10	82	1.11	7.81	329	0.56	60.5
50	54	1.12	7.47	204	0.57	59.5

[a] N is the number of beads in each system.

TABLE 3: Number of Critically Damped or Overdamped Langevin Modes for Different Solvent Viscosities

η (cp)	8LYZ (774 modes)	1VOM (4380 modes)	1Q5G (4620 modes)
0	12	12	12
0.01	90	814	854
0.1	696	3982	4206
0.5	766	4320	4558
1.0	774	4370	4610

become slightly nonmonotonic and sensitive to structure for translation, and wildly nonmonotonic and very sensitive to structure for rotation. In contrast, the results for the R−P tensor smoothly cross a value of $D_{calc}/D_{expt} = 1$ at approximately 6 Å for both translation and rotation and with essentially no variation among the three structures. Results for Mb and Hb with the R−P tensor (bottom two panels) are similar to those for lys, with the optimal bead radii for translation and rotation of 5 and 6 Å, respectively. Because internal modes of a protein are arguably closer in character to rotation than to translation, a bead radius 6 Å is adopted for most of the calculations presented here. Values of the translation diffusion constants, D_t, and rotational relaxation times, τ_{iso}, for the three proteins are listed in Table 1; $\tau_{iso} = 1/6D_r$, where D_r is 1/3 of the trace of the rotational diffusion tensor.

Only beads near the surface of a rigid object contribute to the translational and rotational friction constants; that is, those buried in the center are shielded and can be ignored.[30] To illustrate this effect for the present systems, the accessible surface area (ASA) of each 6 Å bead in lysozyme and myosin (1VOM) was evaluated. C_α whose ASA was 0 Å^2, ≤ 10 Å,^{2} and ≤50 Å^2 were assigned a friction constant of zero to yield three groups. Table 2 shows the results for lysozyme and myosin for the preceding groups and the no-cutoff case. Even at the highest cutoff for lysozyme (60% of beads removed), D_t decreases by only 2% and τ_{iso} increases by 8%. For myosin, these differences are 1 and 3% when almost 75% of the beads are removed.

3.2. Results for Lysozyme and Myosin. Langevin mode calculations were run for 1VOM, 1Q5G, and 8LYZ and were computed at a variety of different solvent viscosities from 0 to 1 cP, as shown in Table 3. This table shows the number of overdamped modes for each structure as solvent friction increases. At zero friction, there are precisely 12 modes with zero eigenvalues; these correspond to the purely translational and rotational motions of the structure. As friction increases, the modes become critically damped, and then overdamped. When a mode becomes critically damped its eigenvalue becomes real. Above 0.1 cP, the vast majority of modes are overdamped, and at 1 cP, all lysozyme modes and all but a very few of the myosin modes follow this pattern.

Because the model used is coarse-grained, many degrees of freedom are eliminated, including those existent entirely within

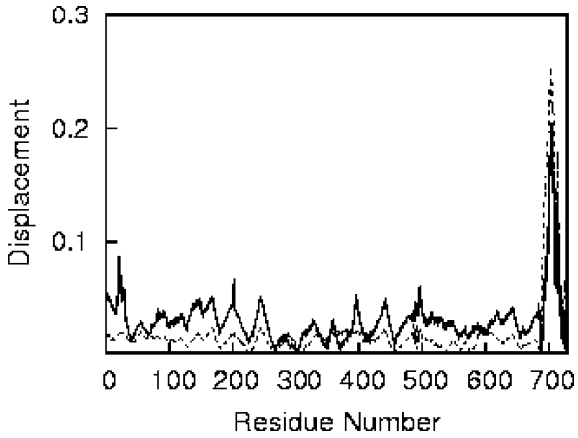

Figure 3. The displacement of the 730 residues of 1VOM for zero-friction elastic network model mode 1 (dotted line) and the displacement portion of the corresponding Langevin network model 10 (solid line).

TABLE 4: Highest Overlap Scores and Corresponding Langevin Mode Number for the Lowest 10 Modes of 1VOM at 1 cP

	1VOM		1Q5G	
ENM mode	highest overlap	Langevin mode	highest overlap	Langevin mode
1	0.8023	10	0.7796	51
2	0.7455	13	0.6493	22
3	0.8628	7	0.5005	8
4	0.5521	11	0.5194	9
5	0.4893	19	0.4217	15
6	0.6751	14	0.4011	18
7	0.4782	15	0.5416	10
8	0.4344	109	0.5127	2325
9	0.4046	32	0.3807	28
10	0.4459	89	0.4543	42

a given residue. This eliminates some very high-frequency modes from the system. In an all-atom approach, it is probable that a higher percentage of modes would remain underdamped at a given viscosity level. However, as reported by Kottalam and Case, above a certain level of friction, almost all low-frequency modes will become overdamped. Therefore, this result indicates that the long time-scale dynamics of lysozyme and myosin are strongly affected by solvent friction, as is expected.

As in the case of lysozyme, the results indicate that a significant number of residues become overdamped, even at relatively low friction, meaning that motion is appreciably affected by the presence of solvent. An interesting question that arises from this basic result is how much the motion described by a given mode changes as friction increases. The mechanism proposed by Brooks and described above was employed to analyze similarities between modes. Because there are many modes to consider and it is difficult to determine a priori which ones are significant, a reliable averaging method would be difficult to construct, and thus, a dot product matrix showing the overlap of all Langevin modes with the 10 lowest-frequency ENM modes was generated. The highest overlapping Langevin modes for 1VOM and 1Q5G are listed in Table 4.

The question of exactly what the highly correlated Langevin mode represents now arises. Zheng and Brooks show that ENM mode 1 of 1VOM is largely a descriptor of the large rotation of the myosin converter.[14] Figure 3 shows the values of the length 3N position vector of this mode versus the zero-friction mode 1 vector and also highlights the most displaced C_α. It is immediately apparent from this figure why there is such a high overlap between these two modes. The effect of friction on the motion is visible in the difference between displacement magnitude of the highly displaced and less displaced residues decreasing from the ENM mode to the Langevin mode. The figure also demonstrates that the most displaced residues are those on the converter, showing that these centers move the farthest, as would be expected in a rotational swing motion. Therefore, the properties of the Langevin mode, which correlates heavily with ENM mode 1, describe the behavior of this motion in the presence of solvent. Large displacements become muted, and some residues that are less displaced at zero friction become modestly more so, since the entire mode remains normalized. This is the result of interaction between myosin and the surrounding solvent, and the degree to which the zero-friction motion is affected by these forces depends on the conformation of the solvent and its velocity.

TABLE 5: Total Absolute Overlap between the Most Significant Langevin Modes and *All* Elastic Network Model Modes at 1 cP

1VOM			1Q5G		
ELM mode	top 5 overlaps	top 10 overlaps	ELM mode	top 5 overlaps	top 10 overlaps
10	0.988	0.999	51	0.878	0.921
13	0.947	0.986	22	0.822	0.913
7	0.950	0.983	8	0.948	0.995
11	0.928	0.990	9	0.949	0.991
19	0.822	0.926	15	0.737	0.872
15	0.896	0.961	18	0.751	0.899
14	0.776	0.898	10	0.830	0.891
109	0.658	0.738	2325	0.678	0.762
32	0.678	0.833	28	0.632	0.810
89	0.697	0.801	42	0.737	0.850

The method of using dot products to generate overlap scores as implemented in Table 4 gives a reasonable method for judging the relative effects of solvent on the motion of various ENM zero-friction modes. The Langevin modes that have the highest overlap scores when compared to ENM modes 1, 2, 3, and 6 have higher overlaps than those that correlate well with the other low-frequency, zero-friction modes. This indicates that the directions of motions represented by these zero-friction modes are not changed as much when solvent viscosity increases as those motions described by other modes such as mode 10.

Another important result is that the low-frequency modes of 1VOM correspond to Langevin modes with noticeably higher overlaps than those associated with the corresponding 1Q5G zero-friction modes. This conclusion is somewhat surprising because 1Q5G appears more compact than 1VOM, and therefore, individual domains would be less affected by friction. It seems likely, however, that since 1VOM has the myosin converter primed for the power stroke, there is a significant internal force driving the low-frequency modes. As the arm swings down, this force, though damped, is not dissipated into other degrees of freedom. In the 1Q5G case, the swinging motion has already largely completed, and myosin is in a "closed" state with the converter arm docked to the rest of the motor domain. It may be that the 1Q5G modes are more susceptible to mixing because 1Q5G is in a "closed" state with the converter docked to the rest of the motor domain.

It is also necessary to confirm that these Langevin modes do not overlap substantially with other zero-friction modes. Because normal modes form a mutually orthogonal basis set, it is possible for a single Langevin mode to overlap significantly with many zero-friction modes. Table 5 shows the sums of correlations from the Langevin modes in Table 1. This shows that the highly overlapping Langevin modes for 1VOM overlap primarily with a single zero-friction mode, and therefore, their motion is close

TABLE 6: Relaxation Times (ns) of the Langevin Mode Most Closely Overlapping with the Elastic Network Model Mode 1 for Myosin (1VOM) and Lysozyme (8LYZ) at Different Viscosities

h (cp)	8LYZ	1VOM
0.01	0.005	0.015
0.1	0.022	0.234
0.5	0.108	1.178
1.0	0.217	2.356

TABLE 7: Relaxation Times (ps) and Overlap Scores for the LNM Mode Most Overlapping with ENM Mode 1 of Lysozyme Where C_α with Accessible Surface below the Cutoff (Å^2) Were Assigned a Zero Friction Constant. N Is the Number of Beads in Each System.

cutoff	N	relaxation time (ps)	overlap score
no cutoff	129	216	0.80
0	92	201	0.82
10	82	191	0.84
50	54	174	0.83

to that of the original zero-friction model. For 1Q5G, there is more mode mixing, although not significantly so for some modes. The conclusion that can be drawn from this is that although the motion of mode 1 in 1VOM may be slowed by friction, the directional characteristic of the motion changes relatively little. This result is not obtained for the 1Q5G structure, indicating that the motion of the lever arm of myosin may be especially designed to be efficient because it does not mix up among many Langevin modes as much as other motions do. Mode 3, which has the highest overlap score, has a large number of motions in the converter, which may be caused by missing residues in this part of the structure.

As stated by Kottalam and Case,[19] it is possible to construct the Langevin mode relaxation time for a particular mode by inverting the real part of its eigenvalue. Table 6 shows that at 1 cP, the damping time of myosin is ~2.35 ns and that for lysozyme is ~0.21 ns. The difference in these two figures is reasonable given that the myosin structure is much larger than lysozyme. It is not appropriate, in this instance, to directly compare ENM mode 1 of 1Q5G because it represents a motion that is different from mode 1 of 1VOM. Instead, Figure 4 shows the relaxation times of the Langevin modes that best overlap the first 10 ENM modes for both 1VOM and 1Q5G. This shows that in general modes for 1Q5G relax more quickly than those of 1VOM. Given that 1Q5G has more highly dissipated Langevin modes, it is possible that the system is designed to trade intact motion for quicker relaxation. Also note in Figure 4 that mode 3 for 1VOM has a significantly longer relaxation time than all other nontranslational and nonrotational degrees of freedom. As stated above, this mode is largely internal to the converter and may represent looseness of the converter subdomain, causing very local motions to be heavily damped by the presence of friction. To verify that the removal of buried residues does not affect these results, the LNM modes for lysozyme were calculated with the friction-buried beads set to zero using the same criteria as applied to overall translation and rotation (Section 3.1, Table 2). The results are shown in Table 7 and indicate that for translation and rotation, buried residues do not substantially affect the results of the simulation. These results are consistent with those shown in Table 2

3.3. A Four-Bead Model. To facilitate a basic understanding of Langevin modes, a four-bead, two-dimensional model is used to represent a lever arm or strained pendulum. More generally, it is useful to consider the variations in a simple model as a function of viscosity. Four different four-bead models, which

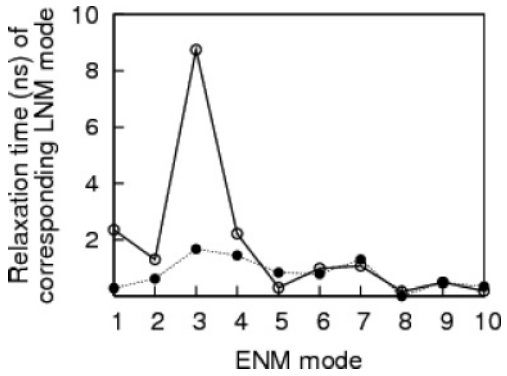

Figure 4. Relaxation times of the Langevin network model modes that overlap with the 10 lowest frequency Elastic network model modes for 1VOM (dark line with open circles) and 1Q5G (dashed line with dark circles).

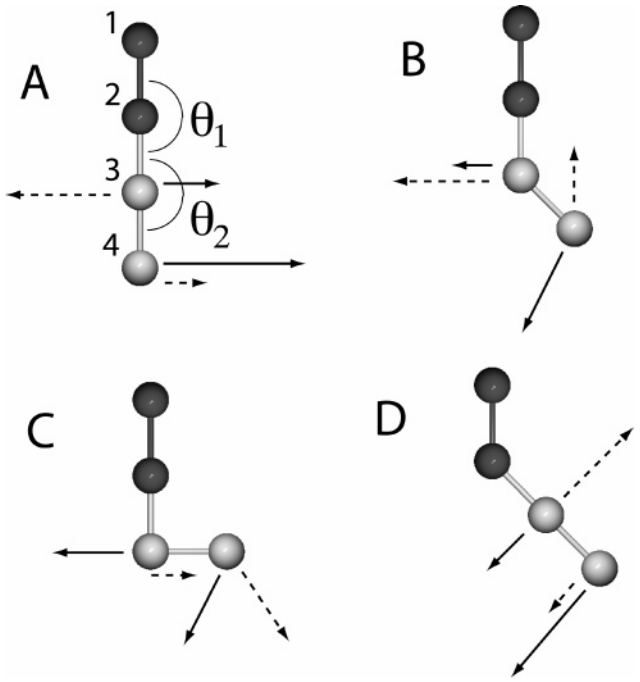

Figure 5. Four different conformations of the four bead model: (A) $\theta_1 = \theta_2 = 180°$; (B) $\theta_1 = 180°$, $\theta_2 = 135°$; (C) $\theta_1 = 180°$, $\theta_2 = 90°$; and (D) $\theta_1 = 135°$, $\theta_2 = 180°$. Beads restrained in all three dimensions are dark-colored; those restrained in only the out-of-plane direction are light colored. Solid arrows show the direction and approximate magnitude of motion of normal mode 1; dashed arrows show the same for normal mode 2.

vary only in the bond angles θ_1 and θ_2, are considered (Figure 5). The four pairs of angles used are 180°−180° (A), 180°−90° (B), 180°−135° (C), and 135°−180° (D). In each case, all beads were separated by 10 Å and assigned a hydrodynamic radius of 15 Å. This value was chosen because in the lysozyme and myosin models presented above, the hydrodynamic radius is roughly 1.5 times the length of a $C_\alpha - C_\alpha$ bond. Beads 1 and 2 were held in a close-to-rigid state via a harmonic restraint with a force constant of 900 kcal/mol/Å^2, while beads 3 and 4 were permitted to move freely in the *x* and *y* directions. A single bond with a force constant of 100 kcal/mol/Å^2 and ideal length of 10 Å connects adjacent beads. A vibrational analysis of these four models produces 12 normal and 24 Langevin modes. Of the 12 normal modes, the 2 that represent the unfixed beads swinging freely in the *x* and *y* directions have the lowest frequencies. The lowest-frequency mode has beads 3 and 4 moving together, whereas the second lowest has this "arm" bent.

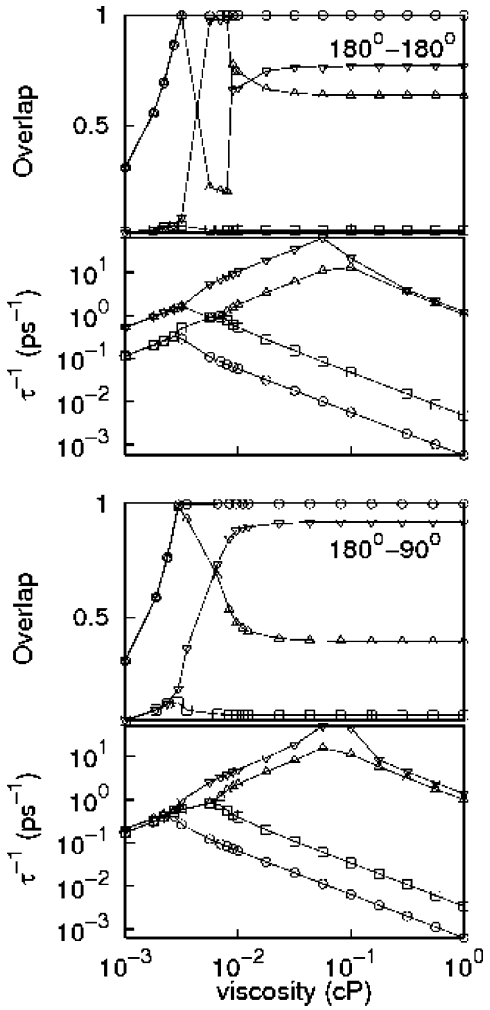

Figure 6. Comparative overlap scores and eigenvalues of the 180°−90° and 180°−180° conformations of the four bead models. The overlap graphs show the scores of LNM mode 1 with ENM mode 1 (○), LNM mode 1 with ELM mode 2 (△), LNM mode 2 with ENM mode 1 (▽), and LNM mode 2 with ENM mode 2 (□). The eigenvalue graphs show the corresponding four lowest eigenvalues.

All of the other normal modes are much higher in frequency due to the restraints placed upon the system.

One question that can be answered by analyzing this structure is how the different conformations affect the amount of mixing of the Langevin modes. It is important to consider how much the coupling of the straight swinging motion with the bending motion of such an exposed domain changes as friction is increased and how the starting conformation of the arm affects this. In this case, conformations A and D have the "arm" extended straight out (collinearly with the remainder of the structure in A and at a 135° angle in D), whereas B and C have it bent at angles of 90° and 135°, respectively. Figure 6 shows how the damping portions of the four lowest Langevin modes overlap with normal modes 1 and 2 as friction is applied. There is a difference in the way the overlaps between the modes cross as viscosity increases. In both cases, the overlap scores of the damping parts increase with friction until the pair of modes overdamps (as is expected). In the case of structure A, however, when the lowest pair splits, the downward sloping eigenvalue line crosses with the splitting of the eigenvalues of the second-lowest pair. That is not the case, however, with C. This leads to a "double crossing" of the overlap scores for A but not for C, therefore indicating that initial conformation plays a role in the ultimate method by which Langevin modes couple as friction is applied. As friction is increased beyond 0.1 cP, the overlap scores do not change appreciably, and the modes of A remain much more highly coupled than those of C.

4. Conclusion

In this paper, we combine the elastic network model techniques with Langevin mode theory to develop the Langevin network model. The method is applied to myosin II. In the action of myosin, any energy introduced into degrees of freedom orthogonal to the power stroke itself likely results in the production of heat. Roughly 60% of the free energy released from the phosphate bond results in the production of heat instead of mechanical work. By examining the Langevin modes of such systems, one can start to address the details of energy loss due to friction. For 1VOM, the critical modes 1 and 2 from the ENM are relatively unperturbed by that addition of friction, other than to provide direct solvent damping. By contrast, with the post-power-stroke 1Q5G structure, there is significant mixing of modes with the addition of friction.

The relaxation times calculated for overdamped LNM modes are all shorter than the translational and rotational diffusion times listed in Table 1. This is because the rotational friction involves all surface residues, whereas a specific Langevin mode involves significant motion only on a subset of surface residues. The relaxation times reported for LNM modes are also significantly shorter than the millisecond time scales for the working stroke. The experimental full cycle time of 5 ms includes numerous steps and reaction barriers, and thus, the times cannot be directly contrasted with a single LNM power stroke result.

Acknowledgment. We thank Attila Szabo for many interesting discussions.

References and Notes

(1) Yamamoto, N. *Teikyo Med. J.* **1999**, *22*, 423.
(2) Kneller, G. *Chem. Phys.* **2000**, *261*, 1.
(3) Lange, O. F.; Grubmüller, H. *J. Chem. Phys.* **2006**, *124*, 214903.
(4) Erkip, A.; Erman, B. *Polymer* **2004**, *45*, 641.
(5) Himmel, D. M.; Gourinath, S.; Reshetnikova, L.; Shen, Y.; Sxent-György, A. G.; Cohen, C. *Proc. Natl. Acad. Sci. U.S.A.* **2002**, *99*, 12645.
(6) He, Z. H.; Bottinelli, R.; Pellegrino, M. A.; Ferenczi, M. A.; Reggiani, C. *Biophys. J.* **2000**, *79*, 945.
(7) Berman, H. M.; Westbrook, J.; Feng, Z.; Gilliland, G.; Bhat, T. N.; Weissig, H.; Shindyalov, I. N.; Bourne, P. E. *Nucleic Acids Res.* **2000**, *28*, 235.
(8) Reubold, T. F.; Eschenburg, S.; Becker, A.; Kull, F. J.; Manstein, D. J. *Nat. Struct. Biol.* **2003**, *10*, 826.
(9) Rüegg, C.; Veigel, C.; Molloy, J. E.; Schmitz, S.; Sparrow, J. C.; Fink, R. H. A. *News Physiol. Sci.* **2002**, *17*, 213.
(10) Navizet, I.; Lavery, R.; Jernigan, R. L. *Proteins* **2004**, *54*, 384.
(11) Tama, F.; Feig, M.; Brooks, C. L., III; Taylor, C. A. *J. Mol. Biol.* **2005**, *345*, 837.
(12) Chennubhotla, C.; Rader, A. J.; Yang, L. W.; Bahar, I. *Phys. Biol.* **2005**, *2*, S173.
(13) Zheng, W.; Doniach, S. *Proc. Natl. Acad. Sci. U.S.A.* **2003**, *100*, 13253.
(14) Zheng, W.; Brooks, B. R. *Biophys. J.* **2005**, *89*, 167.
(15) Zheng, W.; Brooks, B. R. *J. Mol. Biol.* **2005**, *346*, 745.
(16) Zheng, W.; Brooks, B. R.; Thirumalai, D. *Proc. Natl. Acad. Sci U.S.A.* **2006**, *103*, 7664.
(17) Zheng, W.; Brooks, B. R.; Hummer, G. *Proteins* **2007**, *69*, 43.
(18) Lamm, G.; Szabo, A. *J. Chem. Phys.* **1986**, *85*, 7334.
(19) Kottalam, J.; Case, D. A. *Biopolymers.* **1990**, *29*. 1409.
(20) Tirion, M. M. *Phys. Rev. Lett.* **1996**, *77*, 1905.
(21) Brooks, B. R.; Bruccoleri, R. E.; Olafson, B. D.; States, D. J.; Swaminathan, S.; Karplus, M. *J. Comput. Chem.* **1983**, *4*, 187.
(22) Eyal, E.; Yang, L.; Bahar, I. *Bioinformatics* **2006**, *22*, 2619.
(23) Creighton, T. E. *Proteins. Structures and Molecular Properties*; W.H. Freeman and Company: New York, 1984; p 184.
(24) Van Holde, K. E. *Physical Biochemistry* (2nd ed.); Prentice Hall: Englewood Cliffs, New Jersey, 1985, p 117.

(25) Cantor, C. R.; Schimmel, P. R. *Biophysical Chemistry, Part II: Techniques for the Study of Biological Structure and Function*; W.H. Freeman and Company: New York, 1980; p 584.
(26) Muramatsu, N.; Minton, A. P. *Proc. Natl. Acad. Sci. U.S.A.* **1988**, *85*, 2984.
(27) Buck, M.; Boyd, J.; Redfield, C.; MacKenzie, D. A.; Jeenes, D. J.; Archer, D. B.; Dobson, C. M. *Biochemistry* **1995**, *34*, 4041.
(28) Wang, D.; Kreutzer, U.; Chung, Y.; Jue, T. *Biophys. J.* **1997**, *73*, 2764.
(29) Garcia de la Torre, J.; Bloomfield, V. A. *Q. Rev. Biophys.* **1981**, *14*, 81.
(30) Venable, R. M.; Pastor, R. W. *Biopolymers* **1988**, *27*, 1001.
(31) Rotne, J.; Prager, S. *J. Chem. Phys.* **1969**, *50*, 4831.
(32) Brooks, B. R.; Janezic, D;, Karplus, M. *J. Comput. Chem.* **2005**, *16*, 1522.
(33) Humphrey, W.; Dalke, A.; Schulten, K. *J. Mol. Graphics* ***1996***, *14*, 33.
(34) Merritt, E. A.; Bacon, D. J. *Methods Enzymol*. **1997**, *277*, 505.